Integrating Multisensor Satellite Data to Analyze Urban Heat Island and Vegetation Dynamics in Bali

Putu Abel Nugraha Ardyan*, A. Muh. Tegar Juliarga Amrul, and Ilham Alimuddin
Department of Geological Engineering, Faculty of Engineering, Hasanuddin University
Jalan Poros Malino Km. 6, Bontomarannu, Kabupaten Gowa, South Sulawesi, 92171, Indonesia
*abelardyan@gmail.com

Abstract: *Urban heat island (UHI) dynamics in tropical, monsoon-influenced environments require integrated, multi-source observations to capture complex diurnal and seasonal variability. This study integrates MODIS daytime and nighttime land surface temperature (LST), Landsat 8 thermal observations, and Sentinel-2 normalized difference vegetation index (NDVI) to evaluate spatio-temporal patterns of UHI intensity and vegetation dynamics across Bali Province, Indonesia. Two seasonal windows were examined, May to July 2024 (dry season) and December 2024 to February 2025 (wet season) to characterize monsoon-driven contrasts. Satellite-derived thermal and vegetation metrics were processed, analyzed, and mapped across the study area, with key thematic outputs presented as LST and SUHI maps, NDVI distributions, and summary figures. Results show pronounced seasonal contrasts: SUHI signals are weak or slightly negative during the dry season but become strongly positive in the wet season, with localized SUHI values reaching about 9 degrees Celsius in highly urbanized areas. Daytime and nighttime phases exhibit differing responses, underscoring the need to consider both diurnal components. Vegetation consistently moderates surface temperatures, with higher NDVI associated with lower LST, while densely built and coastal zones correspond to higher temperatures, reflecting local controls such as urban morphology, street-canyon effects, and coastal proximity. The multisensor integration reconciles differences in spatial resolution and temporal sampling across platforms, improving spatial coherence of thermal patterns and enabling more reliable detection of spatial hotspots and seasonal shifts that single-sensor analyses may underrepresent. Analytical outputs include composite LST maps, SUHI metrics, NDVI distributions, and comparative summaries that together characterize spatial heterogeneity and temporal dynamics. These consolidated outputs offer practical, data-driven inputs to support monitoring and mitigation of urban heat exposure. Overall, the results demonstrate the value of geospatial data fusion for urban climate diagnostics in monsoon-affected tropical settings and provide an empirical basis to inform climate-sensitive urban planning and vegetation-based mitigation strategies in rapidly urbanizing regions.*

Keywords: Geospatial Data Integration, Multisensor Analysis, Remote Sensing, Urban Heat Island, Vegetation Dynamics

Introduction

Urban growth in Bali has modified the surface energy balance through combined effects of land cover change, building geometry, surface materials, and the reduction of vegetation. These changes tend to increase surface temperature in urban zones relative to their non-urban surroundings, which is observed as the surface urban heat island, that is, the difference between urban and non-urban land surface temperature measured at the same time and within the same region (Oke, 1982; Voogt and Oke, 2003). In humid tropical environments the monsoon cycle, cloud cover, and atmospheric moisture introduce strong seasonal modulation, and the daytime and nighttime behaviors can differ in magnitude and spatial organization (Yamanaka, 2016; BMKG, 2019). A multisensor strategy is therefore necessary. MODIS provides temporally dense daytime and nighttime LST. Landsat 8 provides medium resolution detail to separate urban and non-urban pixels. Sentinel 2 offers spectral sensitivity to vegetation via NDVI. The complementarity among these sensors enables a joint view of thermal patterns and vegetation processes that would be difficult to obtain from a single source (Wan, 2008; Yu et al., 2014; Huete, 2002). Beyond simple data fusion, combining these sensors permits cross validation of seasonal anomalies, separation of signal from cloud or view geometry artifacts, and attribution of spatial gradients to vegetation structure versus surface material properties. Along Bali's coastal and upland transects, mesoscale circulations such as sea and land breezes and orographic modulation can shape thermal contrasts; a multisensor design helps disentangle these mechanisms consistently across spatial scales from roughly 10 to 30 meters for Landsat to 250 meters to 1 kilometer for Sentinel and MODIS, and across daytime and nighttime phases (BMKG, 2019; Yamanaka, 2016; Voogt and Oke, 2003).

This study has four objectives. First, to map the seasonal patterns of daytime and nighttime LST in Bali. Second, to quantify SUHI intensity across seasons and identify its seasonal peak. Third, to evaluate how vegetation relates to LST and SUHI. Fourth, to outline practical implications for monitoring and planning. Two representative seasonal windows are used to highlight monsoon contrast. A longer series from 2020 to 2025 provides background variability. Figures 1 to 4, 6 to 7, and 9 to 10 present thematic maps, Figures 5, 8, 11, and 12 present synthesized graphics, and Tables 1 to 4 summarize key statistics to support an integrated reading of the results (Peng et al., 2012; Zhou et al., 2018). To ensure interpretability and reproducibility, all cross-variable statistics are computed on overlapping valid pixel domains, units are harmonized for LST and SUHI, and correlation outputs are accompanied by confidence information. The workflow is also policy facing: mapped hotspots and temporal

peaks are linked to vegetation shortfalls and built surface characteristics that are amenable to planning interventions, so Figures 1 to 12 and Tables 1 to 4 double as a blueprint for routine monitoring and post intervention evaluation.

Literature Review

Concept and physical basis of SUHI

SUHI reflects differences in surface energy components between urban and non-urban land, namely net radiation, heat storage, conductive and convective heat fluxes, evapotranspiration, and local advection. In surface-energy terms, the urban–non urban contrast can be framed as $Q^* = H + \lambda E + \Delta Q_S + G$, where urban materials typically have lower albedo, higher thermal admittance, and different emissivity, which together increase daytime heat storage (ΔQ_S) and delay nocturnal cooling (Oke, 1982). Urban morphology street canyon aspect ratio, sky view factor, and aerodynamic roughness further modulate radiative trapping and turbulent exchange, often elevating sensible heat (H) while reducing latent heat (λE) because vegetation and soil moisture are limited (Voogt and Oke, 2003). Thermal remote sensing makes it possible to map LST and hence infer SUHI at multiple scales, and to separate daytime and nighttime responses (Oke, 1982; Voogt and Oke, 2003; Zhou et al., 2018). In humid tropical climates, high humidity and frequent clouds suppress daytime heating while also limiting nighttime cooling by increasing downwelling longwave radiation and the effective sky temperature; consequently, nighttime SUHI often appears more organized and spatially coherent than daytime SUHI (Yamanaka, 2016). In maritime settings, land–sea breezes and moist boundary layers can additionally redistribute heat and moisture, reinforcing the seasonal asymmetry between day and night responses (Yamanaka, 2016; Voogt and Oke, 2003).

NDVI and vegetation

NDVI is a normalized difference between near infrared and red reflectance that indicates canopy vigor and fractional cover; it descends from early ERTS and Landsat studies and is implemented operationally in MODIS vegetation index products with quality control and periodic compositing (Rouse et al., 1974; Tucker, 1979; Huete, 2002; Huete et al., 2011). Mechanistically, greener and denser canopies support higher evapotranspiration, shifting available energy toward $\lambda E$and reducing LST, which explains the common negative NDVI–LST relationship (Huete, 2002). However, the sensitivity is not always linear. NDVI can saturate at very high biomass, its signal can be biased by soil background and view–

illumination geometry (BRDF effects), and mixed pixels in peri urban mosaics can blend vegetation with impervious surfaces, weakening apparent relationships at moderate resolutions (Huete, 2002; Huete et al., 2011). Cloud contamination and shadows in the humid tropics also complicate monthly compositing. These considerations imply that NDVI–SUHI links may appear weak when (i) vegetation variability is small, (ii) domain alignment across months/sensors is imperfect, or (iii) urban morphological and material controls dominate the urban–non urban difference (Voogt and Oke, 2003; Zhou et al., 2018). While alternative indices such as EVI were designed to reduce soil and atmospheric effects, NDVI remains widely used because of long archives, algorithmic simplicity, and interoperability with thermal products (Huete, 2002; Huete et al., 2011).

Multisensor integration and anthropogenic proxies

MODIS LST has been widely validated and is routinely used for seasonal and diurnal analyses; Collection 6 products show typical uncertainties on the order of ~1 K under clear skies, adequate for regional SUHI assessment (Wan, 2008; Duan et al., 2019). Landsat 8 TIRS enables medium resolution LST retrieval through split window or single channel methods, commonly paired with NDVI based emissivity estimation; such approaches sharpen the urban non-urban thermal contrast by resolving intra urban patterns but require careful cloud masking and emissivity assumptions (Sobrino et al., 2004; Yu et al., 2014; Du et al., 2015). Cross sensor fusion demands harmonized projections, consistent QA filtering, and domain alignment so that statistics are computed over overlapping valid pixels, a nontrivial step in cloudy, humid regions (Wan, 2008; Duan et al., 2019). Night time lights are commonly used as a proxy of urbanization and human activity intensity, capturing electrification, commercial activity, and transport corridors, although saturation and blooming can complicate interpretation in very bright cores (Elvidge et al., 1997; Ma et al., 2012). Tropospheric nitrogen dioxide columns retrieved by satellite instruments provide an indicator of combustion related emissions and mobility; their spatiotemporal co variation with LST often reflects shared anthropogenic drivers and boundary layer coupling, but meteorological confounders require cautious, contextual interpretation (Krotkov et al., 2016; Silvern et al., 2019).

Global findings on SUHI controls

Comparative and global studies show strong influences of vegetation, albedo, climate regime, and socio-economic factors on both daytime and nighttime SUHI, with clear seasonal variations (Peng et al., 2012; Zhou et al., 2018). Daytime SUHI is often larger in arid or

temperate summers where radiative forcing and vapor pressure deficit are high, whereas nighttime SUHI can be pronounced in humid climates where stored heat is released under atmospheres with higher longwave emissivity (Jin et al., 2005; Zhou et al., 2018). Socio economic indicators population density, infrastructure intensity, and lighting coincide with larger SUHI, but the magnitude and sign can depend on greening policies, surface materials, and building morphology (Peng et al., 2012; Elvidge et al., 1997; Ma et al., 2012). Morphological standardization through the Local Climate Zones framework helps link LST differences to city structure in a comparable manner, enabling intercity benchmarking and clarifying how sky view factor, building height, and surface cover mediate SUHI (Stewart and Oke, 2012; Demuzere et al., 2022). Across studies, strategic urban vegetation, higher albedo materials, and ventilation corridors consistently emerge as levers to mitigate SUHI, though their realized efficacy varies with climate and seasonal moisture availability (Voogt and Oke, 2003; Zhou et al., 2018; Peng et al., 2012).

Methodology

Study area

The study area covers the entire land of Bali and surrounding small islands. Interpretation focuses on the southern urban zone including Denpasar and adjacent districts, since this is the core of human activity and exhibits the most pronounced land cover change. Provincial administrative boundaries are used to clip data, and the regional monsoon provides the seasonal frame (BMKG, 2019; Yamanaka, 2016).

Data and preprocessing

The data set comprises: (i) MODIS daytime and nighttime LST aggregated to monthly composites, (ii) Landsat 8 OLI TIRS for medium resolution LST over urban and non-urban pixels, and (iii) Sentinel 2 NDVI aggregated to monthly composites. A multivariable monthly series from 2020 to 2025 contains LST, NDVI, rainfall, nitrogen dioxide, and night time lights for contextual analysis. All layers are kept at native resolution, reprojected to a common coordinate system, clipped to the administrative boundary, grid aligned, and subject to sensor specific quality control. Rows with anomalous zeros in the long series are excluded from statistics. Sentinel error values such as very large negative placeholders in Landsat derived LST are identified and removed from all calculations (Wan, 2008; Duan et al., 2019; Yu et al., 2014).

Urban and non-urban definition

The urban layer is constructed from an official built up land cover map, then binarized into urban and non-urban. Because the built-up variable in the long series is constant, it is not used for cross month comparison. To reduce misclassification along edges, a one-pixel erosion is applied to the urban boundary prior to extracting statistics. This procedure is consistent with common practice in SUHI studies using medium resolution rasters where edge pixels tend to be mixed (Stewart and Oke, 2012; Zhou et al., 2018).

Seasonal composites and metrics

Two seasonal composites represent the monsoon contrast. The dry season covers May, June, and July 2024. The wet season covers December 2024, January 2025, and February 2025. NDVI is computed from the ratio of the difference and the sum between near infrared and red bands. SUHI in degrees Celsius is defined as the average urban LST minus the average non-urban LST. For the six months, we report the mean, minimum, and maximum of SUHI, daytime LST, nighttime LST, and NDVI. The long series is summarized for the two seasonal windows in terms of average LST, average NDVI, and average rainfall. Numerical summaries appear in Tables 1 to 4, while thematic maps and supporting graphics appear in Figures 1 to 12 (Peng et al., 2012; Huete, 2002; Yu et al., 2014).

Statistical analysis and sensitivity test

Pearson correlation is used to assess NDVI versus daytime LST, NDVI versus nighttime LST, NDVI versus urban LST, NDVI versus non-urban LST, and NDVI versus SUHI across the six months. We report r, p value, and a confidence interval. For context over 2020 to 2025, we compute correlations between LST and rainfall, LST and nitrogen dioxide, LST and night time lights, and NDVI and rainfall. A simple sensitivity test is carried out on the urban definition by eroding and dilating the urban mask by one pixel to measure the influence of boundary uncertainty on SUHI (Stewart and Oke, 2012; Zhou et al., 2018).

Quality assurance and reproducibility

Invalid values, problematic pixels, and outcomes from cloud masking are documented in a quality appendix. All cross-variable statistics are computed only on the pixelwise intersection of valid masks and common months to prevent sample size drift. Sensor specific QA flags are honored, and negative placeholders, saturated returns, and mixed cloud edge pixels are excluded. Native spatial resolution is preserved; where alignment is required, layers are

reprojected to a common CRS and snapped to a shared grid using nearest neighbor to avoid value smoothing. The computational environment, versioned scripts, and parameter files are archived and time stamped to enable exact reproduction. Data sources and algorithm references are listed in the bibliography (Wan, 2008; Duan et al., 2019; Yu et al., 2014; Huete, 2002).

Results and Discussion

Six-month overview and seasonal contrast

Table 1: Monthly summary of daytime and nighttime LST, urban and non-urban LST, SUHI, and NDVI in Bali (May 2024 - February 2025).

Month	Year	LST Day M	LST Night M	LST Urban M	LST Non-Urban M	SUHI	LST L	NDVI
May	2024	25.945	20.517	25.913	25.984	-0.071	20.661	0.449
June	2024	24.842	19.996	24.432	24.944	-0.512	25.655	0.438
July	2024	24.946	19.78	24.654	25.261	-0.607	26.026	0.437
December	2024	27.018	23.269	30.5	24.904	5.596	18.443	0.394
February	2025	26.293	16.865	29.635	24.616	5.019	-9,999	0.44
January	2025	26.713	20.576	32.373	23.363	9.01	29.831	0.465

Source: Authors

Table 1 summarizes the six observed months and displays a consistent seasonal pattern. In the dry season of 2024, daytime LST shows a more uniform warming background over land with warm anomalies in the southern urban cluster. In the wet season of 2024 to 2025, the pattern shifts. A south to center gradient emerges, reflecting orography, vegetation distribution, and a more humid atmosphere. Within this framework, average SUHI is small and can be slightly negative in the dry season, then it strengthens in the wet season and peaks in January 2025. The sign change from negative to positive is evident in Figure 5, which shows monthly SUHI across the six snapshots and allows readers to follow the seasonal transition visually (Peng et al., 2012; Yamanaka, 2016). The daytime LST map for the wet season in Figure 1 highlights hot pockets in the south that track the density of built land. The daytime LST map for the dry season in Figure 2 shows a more uniform warming background, yet the urban to non-urban contrast is still discernible. On wet season peaks, clouds and water vapor tend to suppress daytime maxima. Local clear sky windows, however, can still produce urban hotspots. The contrast between the dry and wet composites is confirmed by statistics in Table 2 (Jin et al., 2005; BMKG, 2019). Nighttime LST in Figure 3 for the wet season exhibits a more pronounced urban to non-urban difference compared with Figure 4 for the dry season. This is consistent

with a humid atmosphere that limits longwave radiative cooling and slows the release of stored heat from surfaces. Additionally, enhanced atmospheric emissivity and weaker nocturnal ventilation under humid monsoon conditions reduce net longwave losses and suppress sensible heat flux from impervious fabrics, allowing urban canyons and high thermal inertia pavements to retain and reradiate energy into the boundary layer through the night, thereby amplifying surface contrasts relative to vegetated surroundings (Voogt and Oke, 2003; Yamanaka, 2016). Together with the reduced sky view factor in dense districts, longwave radiative trapping increases multiple reflections and the effective path length, reinforcing after-sunset warming.

Table 2: Seasonal statistics of SUHI daytime LST nighttime LST and NDVI in Bali (Dry 2024 and Wet 2024 - 2025).

Variable	Dry Season Mean	Dry Season Min	Dry Season Max	Wet Season Mean	Wet Season Min	Wet Season Max
SUHI	-0.397	-0.607	-0.071	6.542	5.019	9.010
LST Day	25.244	24.842	25.945	26.675	26.293	27.018
LST Night	20.098	19.780	20.517	20.237	16.865	23.269
NDVI	0.441	0.437	0.449	0.433	0.394	0.465

Source: Authors

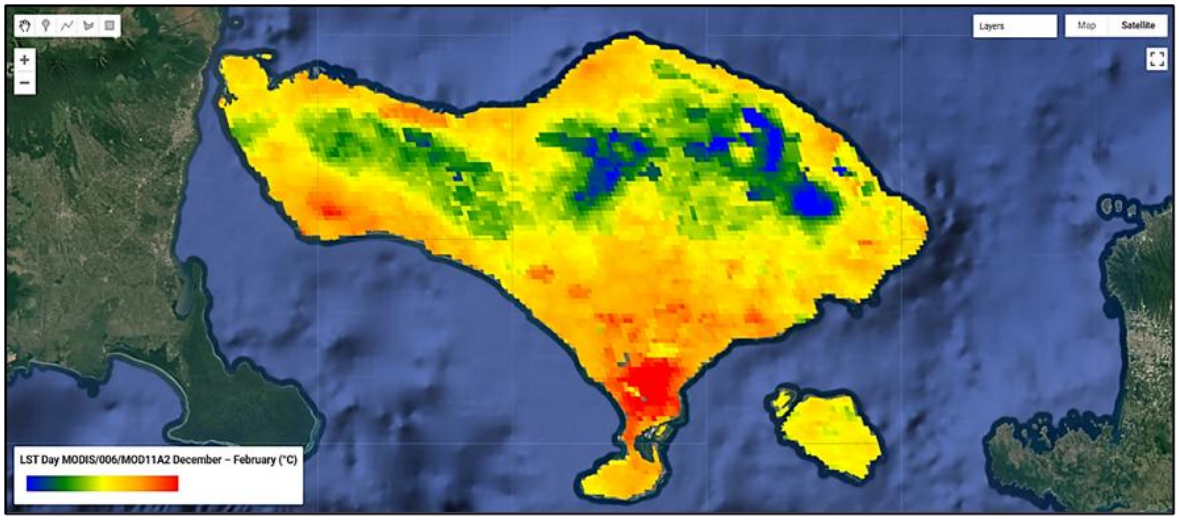

Source: Authors

Figure 1: Daytime land surface temperature (LST) during the wet season (degrees Celsius). Warmer values are concentrated in southern Bali.

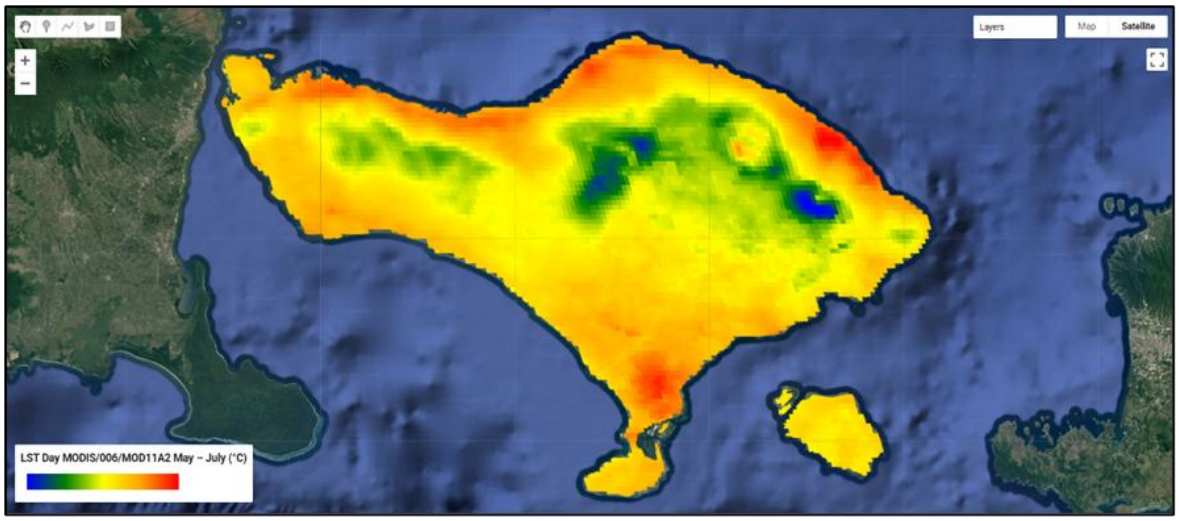

Source: Authors

Figure 2: Daytime LST during the dry season (degrees Celsius), showing cooler pockets that follow the central mountain range.

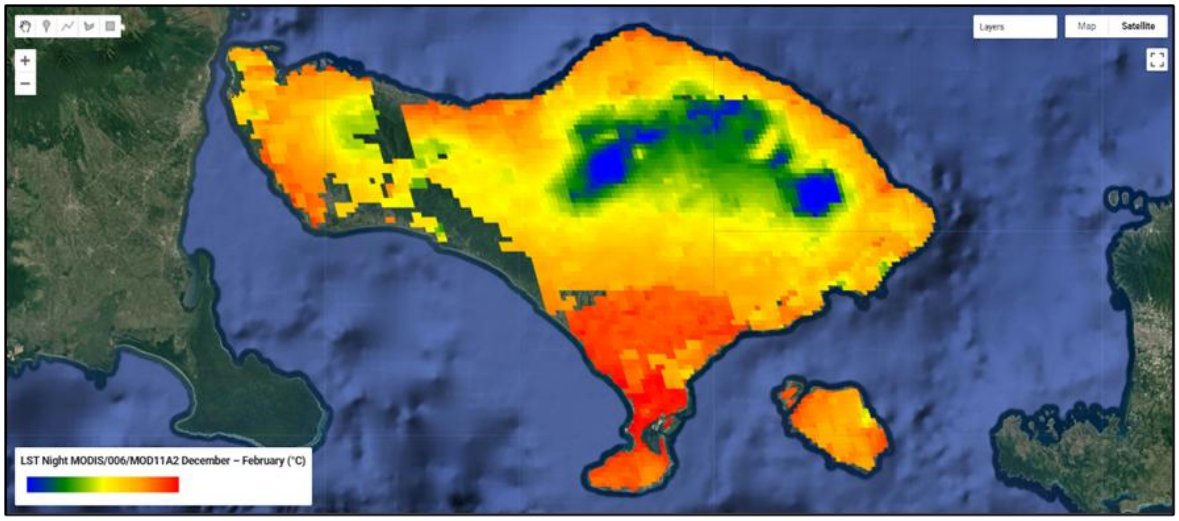

Source: Authors

Figure 3: Nighttime LST during the wet season, with southern Bali remaining warmer than the central highlands.

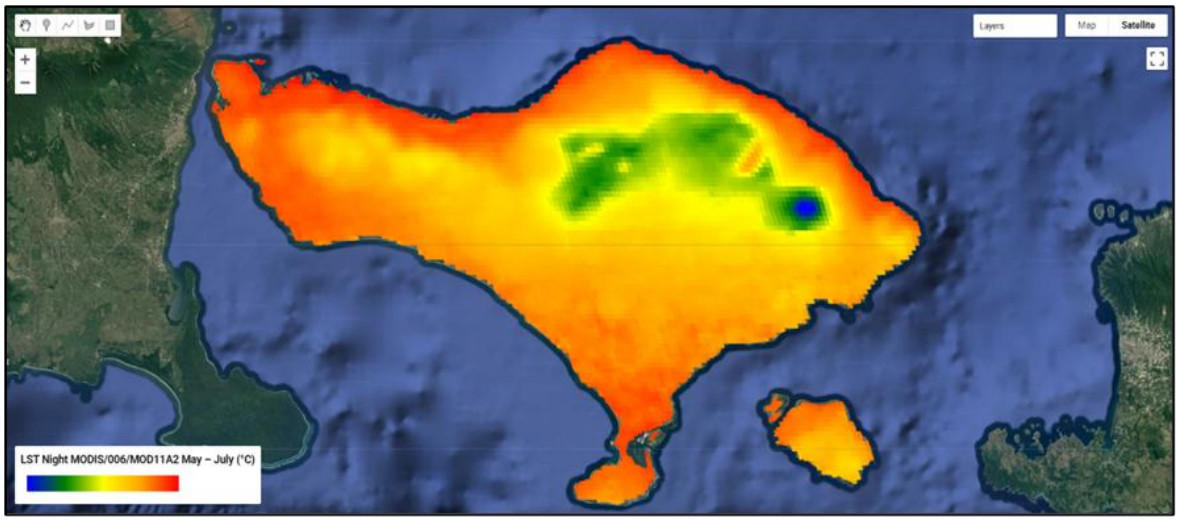

Source: Authors

Figure 4: Nighttime LST during the dry season; the south to north contrast is still visible but weaker.

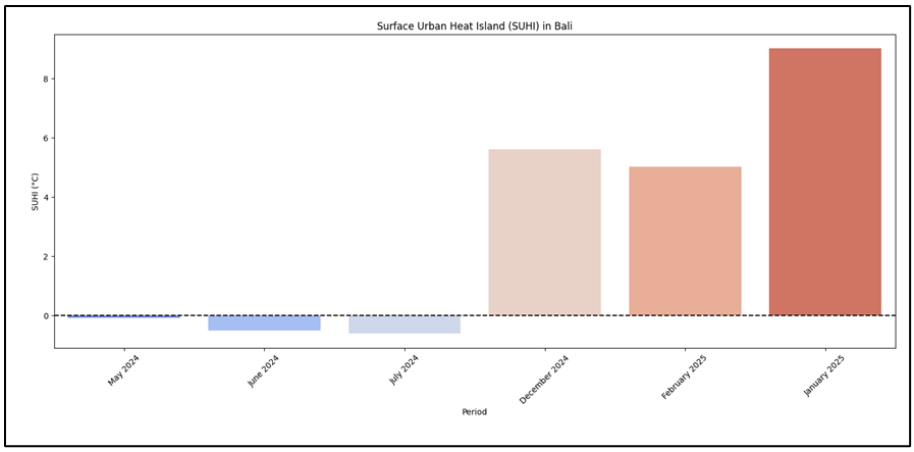

Source: Authors

Figure 5: Monthly SUHI with a zero reference line to highlight sign changes.

Vegetation patterns and implications

The NDVI map for the wet season in Figure 6 displays greater heterogeneity due to cloud influence and soil moisture variability, particularly in the central mountains and the eastern sector. The NDVI map for the dry season in Figure 7 tends to show increased values in many land areas due to reduced cloudiness and stronger shortwave radiation. In general, vegetation acts as a thermal buffer through evapotranspiration that cools the surface. This sensitivity appears as a negative correlation between NDVI and LST, which is clearer at night. Table 2 shows that NDVI varies between seasons, yet not as strongly as temperature does, suggesting that surface and atmospheric controls beyond vegetation shape SUHI in meaningful ways (Huete, 2002; Voogt and Oke, 2003; Zhou et al., 2018).

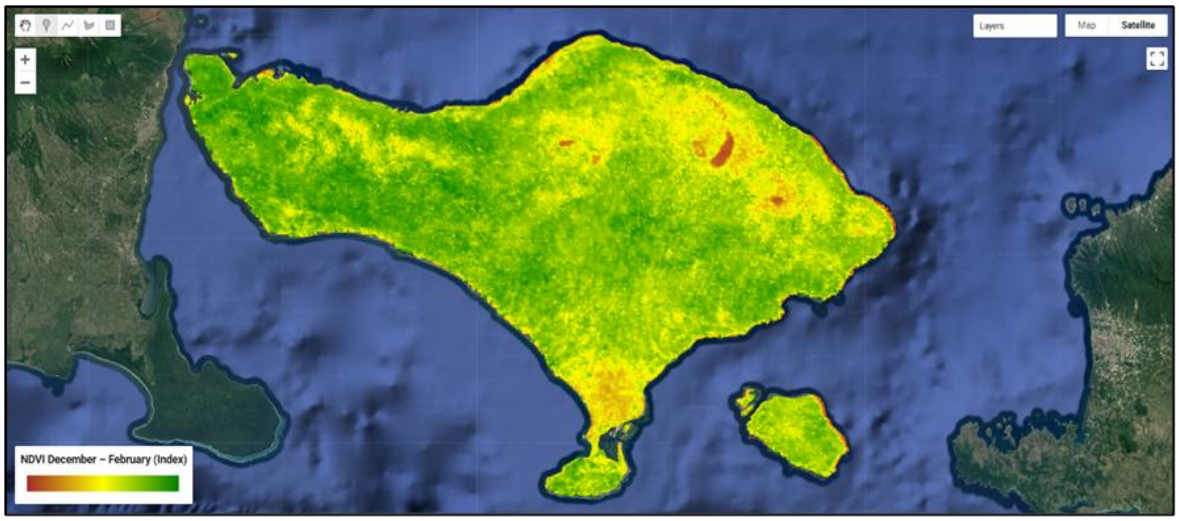

Source: Authors

Figure 6: NDVI during the wet season (unitless index), indicating relatively sparser vegetation in parts of the south.

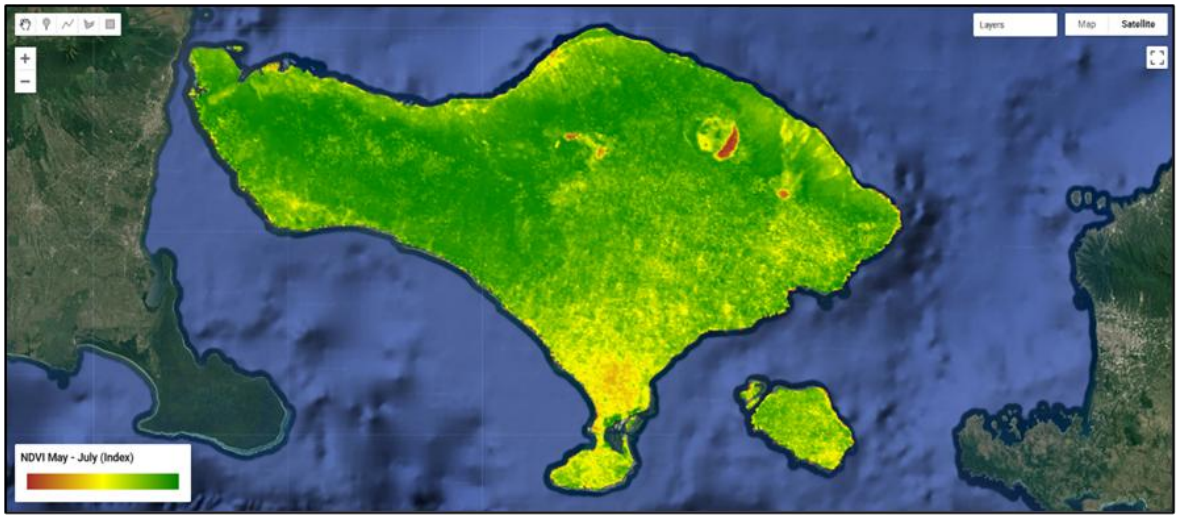

Source: Authors

Figure 7: NDVI during the dry season, with higher values across many land areas, especially in the central to eastern zones.

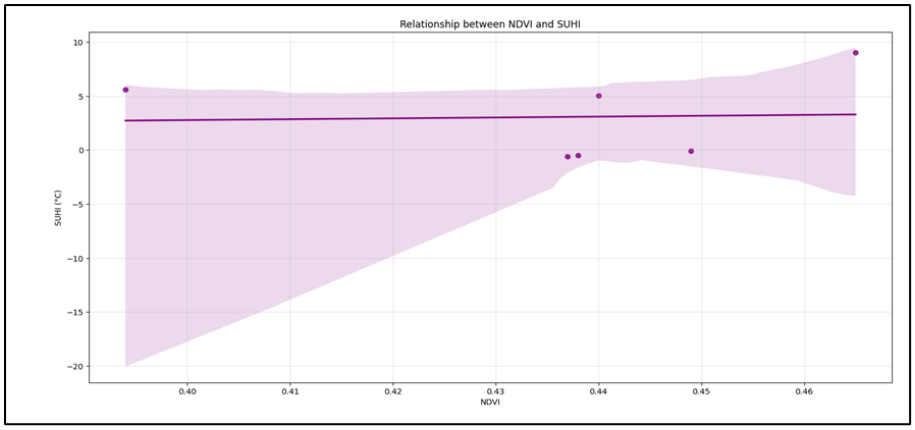

Source: Authors

Figure 8: Relationship between NDVI and SUHI; the shallow slope indicates a weak direct association for the six month sample.

The relationship between NDVI and temperature and the relationship between NDVI and SUHI are further explored in Figure 8, which plots NDVI against SUHI for the six snapshots. The scatter shows a tendency toward a weak to moderate negative correlation, especially in non-urban backgrounds where NDVI increases coincide with lower SUHI. This supports the idea that vegetation contributes to nighttime cooling through residual evapotranspiration and soil water storage that releases moisture to the boundary layer. In dense urban domains, the NDVI influence on SUHI may be masked by urban canyon geometry, low albedo, and materials with high heat capacity. This is why the direct NDVI to SUHI relation is weak in the six-month sample, whereas the NDVI to nighttime LST relation is more consistent, a pattern also visible in the correlation matrix in Table 4 (Stewart and Oke, 2012; Zhou et al., 2018; Peng et al., 2012).

SUHI from thematic maps

The wet season SUHI map in Figure 9 shows positive differences clustered in the southern urban core, while the dry season SUHI map in Figure 10 shows small and mixed differences, including near zero or slightly negative values in peri urban areas. The divergence reflects combined surface and atmospheric effects. When humidity and clouds are higher, nighttime heat loss is reduced, so the heat stored in urban materials is not quickly dissipated. Non-urban surfaces with higher vegetation maintain relatively lower temperatures, widening the urban to non-urban gap. The spatial narrative in Figures 9 and Figure 10 is in line with the SUHI peak in Figure 5 and with wet season statistics in Table 2 that report higher averages than the dry season (Oke, 1982; Voogt and Oke, 2003; Peng et al., 2012).

Long series context in two windows

Table 3: Two seasonal window summaries from the 2020 - 2025 series in Bali (May - July 2024 and December 2024 - February 2025).

Period	Mean LST (°C)	Mean NDVI	Mean Rainfall (mm)
May - July 2024	32.825	0.153	54.562
December 2024 - February 2025	19.947	0.080	711.449

Source: Authors

Table 3 presents the summary of the 2020 to 2025 series for the two windows. In May to July 2024, the background represents the dry season with relatively higher NDVI and lower rainfall. In December 2024 to February 2025, the thermal background decreases in tandem with increased rainfall and humidity. Cross variable correlations in Table 4 show that LST correlates

negatively with rainfall, positively with night time lights, and positively with nitrogen dioxide. NDVI correlates negatively with rainfall. This is consistent with rainfall and clouds reducing temperature, while proxies of human activity co vary with warmer and brighter surfaces (Krotkov et al., 2016; Silvern et al., 2019; Elvidge et al., 1997; Ma et al., 2012).

Table 4: Pearson correlations among key variables from monthly data 2020 - 2025 in Bali.

Variable Pair	r (Pearson)	N (Months)
LST vs Rainfall	-0.564	62
LST vs NO_2	0.388	62
LST vs NTL	0.551	62
NDVI vs Rainfall	-0.572	62

Source: Authors

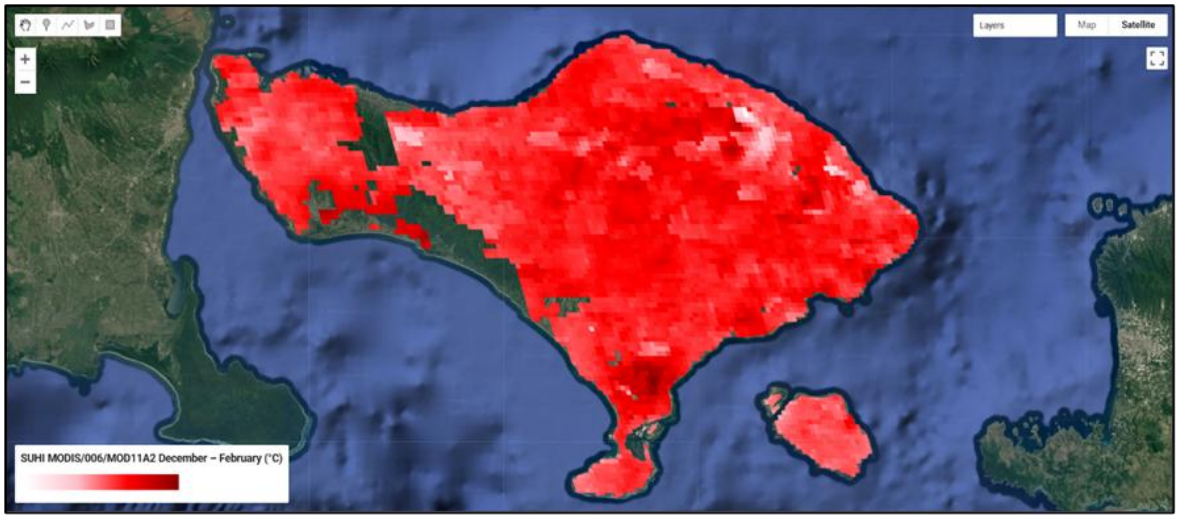

Source: Authors

Figure 9: Surface urban heat island (SUHI) during the wet season, expressed in degrees Celsius and defined as urban LST minus non urban LST.

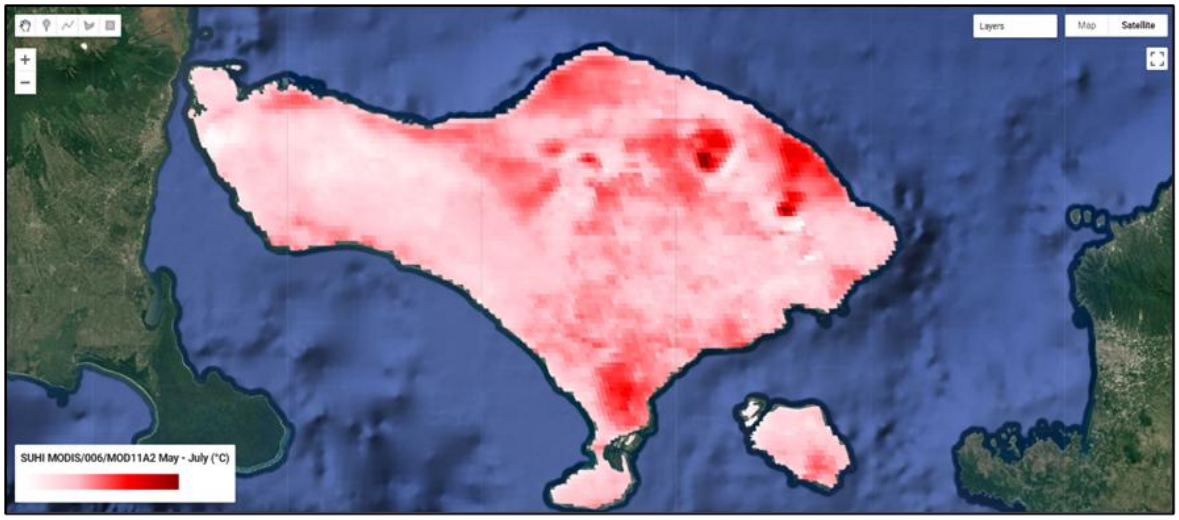

Source: Authors

Figure 10: SUHI during the dry season, showing a weaker urban to non-urban contrast.

Day and night contrast

Figure 11 shows the contrast between daytime and nighttime LST. In the wet season, the distance between the daytime and nighttime curves tends to contract because daytime heating is suppressed by clouds and high humidity, whereas nighttime heat loss is limited by an atmosphere that traps longwave radiation. In energy-balance terms, thicker clouds and higher precipitable water increase downward longwave flux (L↓), raise the effective sky temperature, and reduce the magnitude of net longwave loss ($L^* = L\downarrow - L\uparrow$), so the surface cools more slowly after sunset; at the same time, abundant soil moisture shifts a larger fraction of daytime net radiation into latent heat (λE) rather than sensible heat (H), damping daytime LST variability across land covers. In the dry season, the distance slightly widens because stronger shortwave input and higher vapor pressure deficit amplify daytime heating especially over low-albedo, high heat capacity urban materials while the clearer, drier nighttime atmosphere lowers L↓, enhances radiative cooling, and allows stored heat to be released more efficiently, steepening the day night thermal range. This physical backdrop helps explain why the vegetation signal against nighttime LST is more stable than against daytime LST: at night, confounding shortwave effects and shading are absent, the background is more homogeneous, and contrasts associated with moisture availability and previous-day storage become relatively easier to detect. Consequently, areas with higher NDVI tend to retain more moisture, exhibit greater latent cooling and lower thermal diffusivity, and thus register cooler nighttime surfaces compared with sparsely vegetated or impervious zones patterns that align with the correlation tendencies summarized in Table 4. Taken together, the monsoonal modulation of radiation partitioning and atmospheric emissivity provides a coherent mechanism for the contracted curves in the wet season and the expanded curves in the dry season, as well as for the clearer negative association between NDVI and nighttime LST than with daytime LST (Voogt and Oke, 2003; Huete, 2002; Oke, 1982; Wan, 2008; Yamanaka, 2016).

Reading Figures 5, 8, 11, to 12 as a sequence

The sequence arranged from aggregated summaries to component relations. Figure 5 emphasizes the sign change and the increase in SUHI from dry to wet season. Figure 11 shows the daytime to nighttime relationship that underpins the urban to non urban difference. Figure 12 presents monthly NDVI so that the relative stability of vegetation across the six snapshots can be assessed. Figure 18 depicts NDVI against SUHI and clarifies why the direct NDVI to SUHI relation looks weak in a small sample. Together the four panels provide a narrative arc

that links vegetation, surface temperature, and SUHI within a seasonal frame (Peng et al., 2012; Huete, 2002).

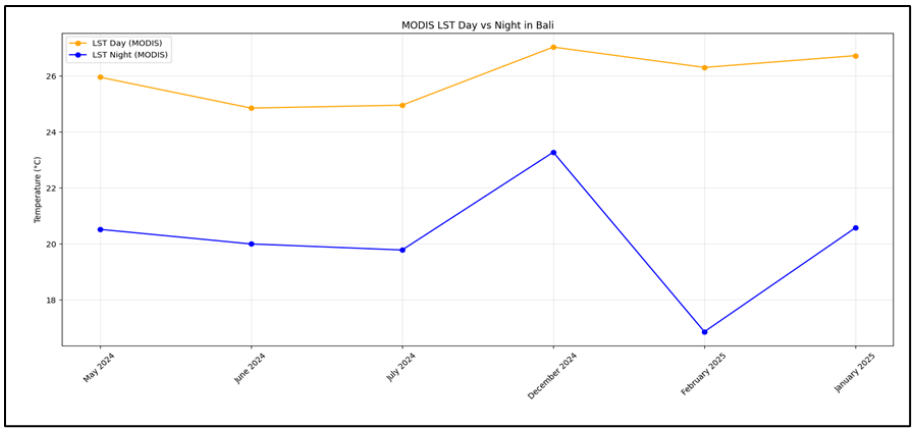

Source: Authors

Figure 11: Contrast between daytime and nighttime LST across the six months.

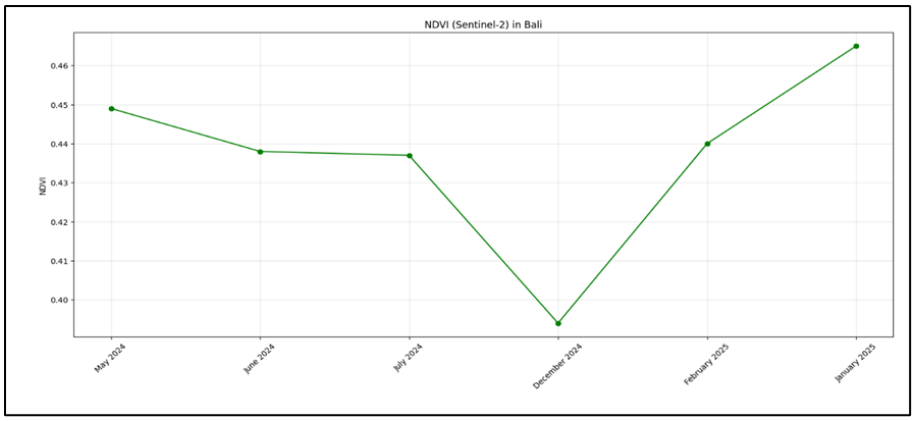

Source: Authors

Figure 12: Monthly NDVI across the two seasonal windows.

Metric consistency and statistical domain

Differences between Table 1 and Table 3 can arise if the domain of valid pixels and the cloud masking rules are not identical. To ensure fair comparison, this study computes all cross variable statistics on the overlapping valid domain only. Visualizations based on data that contain invalid values are moved to a quality appendix so that the main narrative remains clean while transparency is preserved (Wan, 2008; Duan et al., 2019).

Sensitivity test and uncertainty implications

The sensitivity test on the urban boundary using one pixel erosion and dilation shows that SUHI estimates are reasonably stable to small boundary changes. In heterogeneous peri urban mosaics, however, value changes can be larger due to sub pixel mixing. It is therefore advisable to state the urban definition clearly, apply analytical buffers if needed, and report a small

uncertainty band in SUHI when comparing across cities or across long time spans (Stewart and Oke, 2012; Zhou et al., 2018).

Policy and planning implications

The findings argue for a layered cooling strategy. In non urban zones adjacent to the city, increased vegetation cover is effective for nighttime cooling and for stabilizing the thermal background. In dense urban domains, recommended strategies include higher albedo surfaces, materials with lower effective heat capacity, and wind corridors to enhance ventilation. For periodic evaluation, the same multisensor framework can be used as an evidence based monitoring dashboard. Policies that combine vegetation, material, and ventilation approaches are likely to reduce SUHI during wet season peaks as shown by Figure 5, Figure 9, and the statistics in Table 2 (Peng et al., 2012; Stewart and Oke, 2012; Zhou et al., 2018).

Limitations and future directions

The six month composite set is appropriate for highlighting monsoon contrast, but it is not sufficient for very strong statistical claims. Small sample correlations are sensitive to one or two extreme months. In humid tropics, the valid pixel domain can shift between months due to cloud masks, which can alter statistics if not harmonized. Extending the time coverage, enforcing identical domains across sensors, and experimenting with vegetation metrics beyond NDVI, such as EVI or physically based canopy temperature metrics, would help test sensitivity more robustly. Incorporating urban morphology classes, for example Local Climate Zones, would also improve attribution of SUHI differences to specific urban forms (Stewart and Oke, 2012; Huete, 2002; Demuzere et al., 2022; Zhou et al., 2018).

Conclusion and Recommendation

The integration of MODIS, Landsat 8, and Sentinel 2 in the Bali case study successfully captures seasonal dynamics of surface temperature and vegetation. In the dry season of 2024, SUHI is small and can be negative. In the wet season of 2024 to 2025, SUHI increases sharply and peaks in January 2025 in the dense southern urban core. Daytime and nighttime LST show a contrast consistent with the roles of clouds and humidity. NDVI shows a clearer negative relation with nighttime LST than with daytime LST. The direct NDVI to SUHI relation is weak across the six snapshots, which indicates that the urban to non urban difference is influenced by multiple factors beyond vegetation. The two window long series supports the view that rainfall is a first order control, while LST relates positively to night time lights and to nitrogen

dioxide as proxies of human activity and emissions. The thematic maps in Figures 1 to 4, 6 to 7 and 9 to 10, the synthesized graphics in Figures 5, 8, 11 and 12, and the statistics in Tables 1 to 4 provide a coherent and mutually reinforcing account of these results (Oke, 1982; Voogt and Oke, 2003; Peng et al., 2012; Zhou et al., 2018; Wan, 2008; Huete, 2002). Practical implications include three priorities. First, expand vegetation in peri urban belts for nighttime cooling. Second, manage materials and albedo and design ventilation corridors in dense urban domains to reduce heat storage. Third, reuse the same multisensor framework for periodic monitoring so that the effects of interventions can be evaluated objectively over time. Future work should broaden temporal coverage, enforce identical valid domains across sensors, and explore additional vegetation and morphology metrics to assess SUHI sensitivity with a wider and more diverse evidence base (Stewart and Oke, 2012; Yu et al., 2014; Demuzere et al., 2022).

Acknowledgments

We thank to Mr. Ilham Alimuddin as the supervisor and colleagues at the Department of Geological Engineering, Universitas Hasanuddin, for feedback during the preparation of this research, and the providers of open satellite data products that made this seasonal province scale analysis feasible.

References

BMKG. (2019). *Climate Variability of Indonesia*. Badan Meteorologi, Klimatologi, dan Geofisika.

Demuzere, M., et al. (2022). A global map of local climate zones to support earth system modelling and urban climate research. *Earth System Science Data*, 14, 3835–3873.

Du, C., Ren, H., Qin, Q., Meng, J., & Zhao, S. (2015). A practical split-window algorithm for estimating land surface temperature from Landsat 8 data. *Remote Sensing*, 7(1), 647–665.

Duan, S.-B., Li, Z.-L., Li, H., et al. (2019). Validation of Collection 6 MODIS land surface temperature product. *Remote Sensing of Environment*, 225, 18–29.

Elvidge, C. D., Baugh, K. E., Kihn, E. A., Kroehl, H. W., & Davis, E. R. (1997). Mapping city lights with nighttime data from the DMSP Operational Linescan System. *Photogrammetric Engineering & Remote Sensing*, 63(6), 727–734.

Huete, A. (2002). Overview of the radiometric and biophysical performance of the MODIS vegetation indices. *Remote Sensing of Environment*, 83(1–2), 195–213.

Huete, A., Didan, K., Miura, T., Rodriguez, E. P., & Gao, X. (2011). MODIS Vegetation Indices. In *Remote Sensing Time Series*. Springer.

Jin, M., Dickinson, R. E., & Zhang, D. (2005). The footprint of urban areas on global climate as characterized by MODIS. *Journal of Climate*, 18(10), 1551–1565.

Krotkov, N. A., et al. (2016). Aura OMI observations of regional SO_2 and NO_2 pollution changes. *Atmospheric Chemistry and Physics*, 16, 4605–4629.

Ma, T., Zhou, C., Pei, T., Haynie, S., & Fan, J. (2012). Quantitative estimation of urbanization dynamics using DMSP/OLS nighttime light data in China. *Remote Sensing of Environment*, 124, 99–107.

Oke, T. R. (1982). The energetic basis of the urban heat island. *Quarterly Journal of the Royal Meteorological Society*, 108(455), 1–24.

Peng, S., et al. (2012). Surface urban heat island across 419 global big cities. *Proceedings of the National Academy of Sciences*, 109(40), 15314–15319.

Rouse, J. W., Haas, R. H., Schell, J. A., & Deering, D. W. (1974). Monitoring vegetation systems in the Great Plains with ERTS. In *Third Earth Resources Technology Satellite-1 Symposium* (NASA SP-351).

Silvern, R. F., Jacob, D. J., et al. (2019). Using satellite observations of tropospheric NO_2 columns to infer long-term trends in U.S. NOx emissions. *Atmospheric Chemistry and Physics*, 19, 8863–8878.

Sobrino, J. A., Jiménez-Muñoz, J. C., & Paolini, L. (2004). Land surface temperature retrieval from Landsat TM-5 thermal infrared data. *Remote Sensing of Environment*, 90(4), 434–440.

Stewart, I. D., & Oke, T. R. (2012). Local climate zones for urban temperature studies. *Bulletin of the American Meteorological Society*, 93(12), 1879–1900.

Tucker, C. J. (1979). Red and photographic infrared linear combinations for monitoring vegetation. *Remote Sensing of Environment*, 8(2), 127–150.

Voogt, J. A., & Oke, T. R. (2003). Thermal remote sensing of urban climates. *Remote Sensing of Environment*, 86(3), 370–384.

Wan, Z. (2008). New refinements and validation of the MODIS land-surface temperature/emissivity products. *Remote Sensing of Environment*, 112(1), 59–74.

Yamanaka, M. D. (2016). Physical climatology of the Indonesian maritime continent. *Progress in Earth and Planetary Science*, 3, 31.

Yu, X., Guo, X., & Wu, Z. (2014). Land surface temperature retrieval from Landsat 8 TIRS: Comparison among RTE, split-window, and single-channel methods. *Remote Sensing*, 6(10), 9829–9852.

Zhou, D., Xiao, J., Bonafoni, S., et al. (2018). Satellite remote sensing of surface urban heat islands: Progress, challenges, and perspectives. *Remote Sensing*, 11(1), 48.